Chapter 4

RATE ENHANCEMENT FROM CARBONIC ANHYDRASE: MECHANISTIC INSIGHTS FROM IMMOBILIZATION WITHIN CARBON CAPTURE REACTORS

4.1 Introduction

Humans are burning fossil fuels at an unprecedented rate, leading to accelerated melting of polar ice sheets (Chen et al., 2006; Rignot et al., 2011; Velicogna, 2009), acidification of the oceans (Doney et al., 2009; Feely et al., 2012; Zeebe, 2012), and potential increases in the strengths and/or frequencies of hurricanes (Bender et al., 2010; Emanuel, 1987; Knutson et al., 2010; Powell and Reinhold, 2007) and forest fires (Dale et al., 2001; De Groot et al., 2013; Flannigan et al., 2013; Wotton and Flannigan, 1993), among other things. Our unfettered release of CO_2 into the atmosphere is also expected to have grave economic and social consequences (Stern and Stern, 2007; Tol, 2002; Yi, 1996). Climate change represents an existential threat to humanity, but even the major changes to our energy infrastructure set forth in the Paris Climate Agreement are expected to insufficient to keep global warming below 2°C (Rogelj et al., 2016). Any emissions reduction strategy should therefore include a source of negative emissions, i.e. carbon capture and storage technologies, before it is considered viable.

The Earth's oceans will eventually neutralize anthropogenic CO_2 via the dissolution of carbonate minerals, but the natural timescale of this process is far longer (~2000-6000 years) than what is needed to avoid 2°C of global warming (Archer et al., 1998; Archer and Maier-Reimer, 1994; Boudreau et al., 2010; Cao et al., 2009; Ilyina and Zeebe, 2012; Lenton et al., 2006; Ridgwell and Zeebe, 2005; Sundquist, 1990). One proposed strategy is to decouple the timescales of carbonate dissolution and ocean circulation by acidifying reactor vessels with CO_2-rich flue gas (Caldeira and Rau, 2000; Rau et al., 2007, 2001; Rau and Caldeira, 1999). This acidified water could then be used to dissolve carbonates, effectively capturing and storing CO_2 in the form of bicarbonate. This idea has been bolstered by the discovery that an enzyme, carbonic anhydrase (CA), increases carbonate dissolution rates by orders of

magnitude (Dreybrodt et al., 1996; Li et al., 2009; Subhas et al., 2017; Xie and Wu, 2014; Zaihua, 2010).

Carbonic anhydrase is found in nearly all animals and photosynthesizing organisms, and it catalyzes the reversible hydration of carbon dioxide to bicarbonate:

$$CO_2 + H_2O \leftrightarrows H^+ + HCO_3^- \leftrightarrows H_2CO_3 \qquad \text{Eq. (4.1)}$$

The catalytic mechanism of CA involves the attack of a zinc-bound OH^- on a CO_2 molecule captured within a hydrophobic pocket. The resulting HCO_3^- ion is displaced into solution by H_2O, where it rapidly equilibrates with H_2CO_3. The zinc-bound OH^- is regenerated by transferring a H^+ from the newly acquired water molecule onto His-64, which then shuttles the proton onto buffer molecules in solution (Lindskog, 1997).

Though the mechanism of CO_2 hydration by CA is known, the mechanism by which the enzyme enhances carbonate dissolution rates is not. The H^+ generated during the CO_2 hydration process is often thought to be responsible for dissolution enhancement (Dreybrodt et al., 1996; Pokrovsky et al., 2005), but H_2CO_3 is also plausible (Subhas et al., 2017), as it is an important nucleophile in dissolution rate laws (Arakaki and Mucci, 1995; Busenberg and Plummer, 1986; Chou et al., 1989; Plummer et al., 1979b). A detailed study is required to understand the dissolution catalysis of CA, and the results will inform the design of any reactor hoping to harness the catalytic effects of the enzyme. From a practical standpoint, this is because CA must be retained within a dissolution reactor to be economically feasible. The most promising ways to retain CA are by physically trapping the enzyme within porous hydrogels (reviewed in Avnir et al., 1994), or by chemically linking it to controlled pore glass (CPG, reviewed in Weetall, 1993). CA may be physically separated from the mineral if dissolution is catalyzed via an increase in the concentration of carbonic acid in solution. However, if CA catalyzes dissolution via direct proton transfer onto the surface (if the mineral is the “buffer molecule” that accepts the proton from His-64), then a reactor design will need to allow for the intimate association of CA with the mineral surface.

In this chapter, we construct prototype fluidized bed and packed bed carbonate dissolution reactors for use as CO_2 capture and storage devices. We implement methods for retaining CA within hydrogels and on the surface of CPG beads, and we evaluate the resulting effects on the activity and effective lifetimes of the enzyme. Finally, we combine our fixed CA products with our reactors and use the results to understand the mechanism by which the enzyme enhances calcite dissolution rates.

4.2 Methods

4.2.1 Reactor Designs

Dissolution catalysis of crushed carbonate rock was evaluated using both fluidized bed and packed bed reactors. Fluidized bed reactors (Fig. 4.1) were fabricated using 50 cm lengths of clear PVC pipe (McMaster-Carr item #49035K48), ¼" NPT fittings, tygon tubing, polycarbonate powder funnels, and stainless-steel mesh (0.034" pore size, McMaster-Carr item# 85385T91). The base of each reactor was made by cutting a funnel in half, placing stainless-steel mesh in between the newly separated pieces, and epoxying the funnel back together and onto the PVC pipe. After assembly, carbonate rock was poured into the base and a peristaltic pump was used to flow either seawater (starting alkalinity 1900 μmol kg^{-1}) or tap water (starting alkalinity of 1200 μmol kg^{-1}) into the reactor. Excess water drained out of the top port such that the steady volume of each reactor was 300 mL during operation. Dissolution progress was monitored using open-system gran titration to measure the alkalinity of the reactor outflow at regular time intervals. CA was purchased in its lyophilized form from Worthington Biochemical Co. (item # LS001263) and either dissolved directly into the inflow water stream or added in an immobilized form as discussed below.

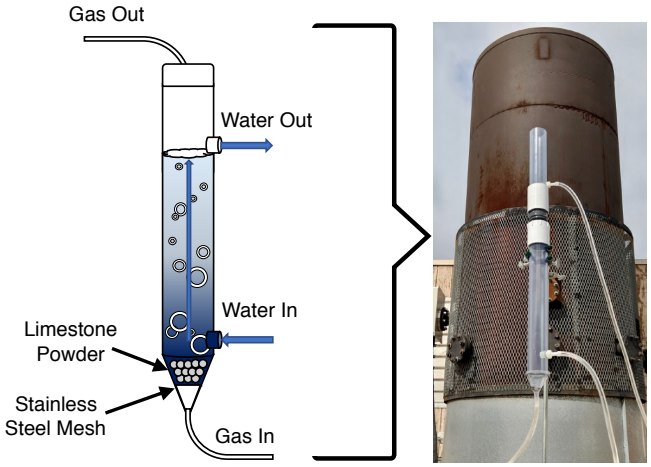

Figure 4.1: Schematic of fluidized bed reactor (left) and full assembled reactor (right)

The reactor carbonate bed was fluidized using either a compressed gas line (10% CO_2, balance N_2) or a diaphragm air pump. The diaphragm pump was used to test dissolution rates when flowing in either ambient air or 3% CO_2 sourced from the Caltech cogeneration powerplant smokestack. To prevent diffusion limitation of the dissolution rate, the minimum gas flow rate required for bed fluidization (u_{mf}, cm s^{-1}) was calculated according to:

$$u_{mf} = \frac{(\Psi d_p)^2}{150\mu}[g(\rho_p - \rho_{fluid})]\frac{\varepsilon^3}{1-\varepsilon} \qquad \text{Eq. (4.2)}$$

Here, Ψ is the sphericity of the particles in the bed (ranging between 0.5 and 1, with 0.6 being typical for a granular solid), d_p is the average diameter of the particles (cm), μ is the viscosity of the inflow gas ($1.86 \cdot 10^{-4}$ g cm^{-1} s^{-1} for air), g is acceleration due to gravity (980 cm s^{-2}), ρ_p is the density of the particles (2.71 g cm^{-3} for calcite), ρ_{fluid} the density of the inflow gas ($1.2 \cdot 10^{-3}$ g cm^{-3} for air), and ε is a measure ranging from 0-1 of the porosity of the particles when fluidized (assumed value of 0.5).

The size fraction of carbonate rock to use in the reactor was chosen with care, as u_{mf} increases with the square of the particle diameter. Large grain rock is most realistic for an industrial application, but given a 3 cm bed diameter (midpoint diameter of the funnel), a 1-

2 mm size fraction required a gas flow rate of ~82 L min^{-1}. Initial experiments used this larger grain size of rock, but the fast flow rate drained a full tank of compressed CO_2 gas within 12 hours, 10 hours of which were required for the alkalinity of the reactor to reach steady state. Later experiments were conducted using a 0.25-0.5 mm rock size fraction because they required a lower gas flow rate (calculated 5.1 L min^{-1}) and could achieve steady state alkalinity more quickly.

Packed bed reactors were made from 30 mL buchner filter funnels with 40-90 μm pore size fritted discs (VWR catalog # 10546-042). Each reactor was filled with 48 g of crushed carbonate rock and topped with a greased rubber stopper that had been threaded with a section of tygon tubing. A larger rock size fraction (1-2 mm) was used because there was a greater chance of observing a catalytic rate enhancement when testing slower dissolution rates. A peristaltic pump was used draw seawater (starting alkalinity 1900 μmol kg^{-1}) from a 4 L reservoir and push it continuously through the packed bed. The seawater was acidified prior to beginning each experiment by bubbling in 10% CO_2 for a minimum of one hour. The reaction progress of the experiment was monitored by measuring the alkalinity of the effluent.

4.2.2 CA Immobilization Strategies

CA was physically trapped within polyethylene glycol diacrylate (PEGDA) hydrogels following the method outlined in Blanchette et al. (2016). Briefly, CA was mixed together with pH 7 phosphate buffer solution, PEGDA macromer, and photoinitiator. The resulting solution was then cured into a solid hydrogel via exposure to UV light. We tested a suite of PEGDA sizes (Laysan Bio Item# ACRL-PEG-ACRL-4MW Kit), PEGDA concentrations, photoinitiators ("2H2M" VWR item #H0991-25G, and "TPO-Li," a proprietary agent from CPS Polymers), and UV intensities ($1 \cdot 10^{-3}$ – 1 W cm^{-2}) to find a combination that optimized CA activity and lifetime (activity measurements detailed in Section 4.2.3) . The UV lamps used were a handheld 365nm lamp ($1 \cdot 10^{-3}$ W cm^{-2}, Fisher Scientific catalog # UVP95000602), a small 405nm lamp (0.6 W cm^{-2}, Peopoly UV curing light), and a 405nm UV flood lamp (1 W cm^{-2}, Loctite IDH: 1359255 for controller, 2139180 for lamp).

Curing times ranged from 5 minutes at the weakest UV intensity to 10 seconds at the strongest. Note that PEGDA macromer comes as a solid powder, so its concentration in solution is defined in terms of weight percentage. For example, 50 mg of PEGDA added to 500 mg of buffer solution is referred to as a 10% PEGDA solution.

Table 4.1: Summary of Hydrogel Materials	
PEGDA MW (g mol^{-1})	575, 5k, 10k, 20k
Photoinitiators	2-hydroxy-2-methylpropiophenone ("2H2M"), TPO-Li
UV lamps	365nm ($1 \cdot 10^{-3}$ W cm^{-2}), 405nm (0.6 W cm^{-2}), 405nm (1 W cm^{-2})

Pure hydrogels were cured into various shapes and evaluated for mechanical robustness and CA activity. Porous silicone sheets (PS sheets) provided by the Baker lab at Lawrence Livermore National Lab were also tested as a material to potentially balance the durability and surface area of the hydrogel. The ~1 mm thick sheets were fabricated according to a proprietary process adapted from previous work (Durban et al., 2018) and were delivered to Caltech in deionized water. The PS sheets were stable for several months. To cure CA-hydrogel within the PS sheet, the sheet was first cut to the desired size (typically 1 cm^2) and then dehydrated by gently patting with a Kimwipe. A 20-50 μL drop of PEGDA-enzyme solution was placed on the sheet and absorbed via capillary action. The PS sheet was then placed under UV light and cured for 10 seconds to 5 minutes, depending upon the UV light intensity.

Through a large amount of trial and error, a research scientist in our group, Dr. Panqing He, adapted previous work (Thakur et al., 2007; Weetall, 1993) to design a method for chemically linking CA to aminated CPG beads. The first step of the process is to exchange the amine groups on the surface of the glass beads with glutaraldehyde (GA) groups. Aminated CPG beads (LGC Biosearch Technologies catalog #BG1-2000-10) were prepared for functionalization by wetting them in a stirred beaker of 70-80°C 18 MΩ cm^{-1} water for 1 hour. Once the beads ceased floating and began to sink, they were heated for an additional 30 minutes and then taken off the hotplate to cool. The beads were subsequently placed in 4-

5 g batches into a lined Buchner funnel and dried under vacuum. In order the replace the CPG amino groups with GA linkers, the beads were rinsed while under vacuum with a 2.5% GA solution made by diluting 50% GA (VWR item #97064-690) with 50 mM pH 7 phosphate buffer solution. 250 mL of 2.5% GA was rinsed over the beads over a 1-hour period.

Once functionalized, the CPG beads were ready to be coupled with CA. A concentrated enzyme solution was created by adding 12 mg of CA to a 0.1 M pH 7 phosphate buffer for every gram of CPG beads to be reacted. The beads and enzyme solution were stirred together in a beaker at room temperature for one hour. 1 mL samples of the enzyme solution were taken at 0, 3, 10, and 60 minutes for later testing of the reaction progress using protein UV absorbance spectroscopy. After reacting for an hour, the beads were filtered from the solution and rinsed under vacuum in a Buchner funnel with 500 mL of 50 mM pH 7 phosphate buffer.

The last step of the process was to block unreacted GA sites on the CPG beads and remove loosely bound CA. The coupled CA-CPG beads were stirred together with a 0.1 M pH 7 glycine solution for 1 hour 45 minutes at room temperature. Loosely bound proteins were then removed from the CPG beads by heating the glycine-CPG solution at 50°C for 30 minutes. Finally, the CA-CPG beads were filtered and stored at 5°C in 50 mM pH 7 phosphate buffer. The amount of CPG-bound CA was estimated from the decrease in UV absorbance at 280 nm of the 1 mL enzyme solution samples. The absorbance typically decreased by ~85% from t = 0 minutes to t = 60 minutes, indicating a maximum loading of ~ 10 mg CA per mg CPG beads.

4.2.3 MIMS Method for CA Activity and Lifetime Measurements

The activities of free CA, CA-CPG beads, and CA hydrogels were evaluated using a Pfeiffer QMG 220 Membrane Inlet Mass Spectrometer (MIMS) following the methods developed by Subhas (2017). In this method, a $H^{13}C^{18}O_3$ isotope spike is injected into pH 8 phosphate buffer solution alongside the desired amount of enzyme, and the activity is determined by the rate of depletion of ^{18}O from aqueous $^{13}CO_2$. The fraction of ^{18}O isotopologues of $^{13}CO_2$ was calculated according to:

$$f^{18} = \frac{2(49)+(47)}{2[(45)+(47)+(49)]} \qquad \text{Eq. (4.3)}$$

Here (45), (47) and (49) are the ion currents measured by the MIMS at those *m*/*z* values. The rate of hydration/dehydration was calculated from the slope of $\ln(f^{18})$ s^{-1} (Mills and Urey, 1940; Silverman and Tu, 1976; Subhas, 2017; Uchikawa and Zeebe, 2012). After an initial equilibration period, $\ln(f^{18})$ s^{-1} decreases linearly in proportion to the activity of CA (Subhas, 2017). A typical activity measurement could be completed in 8-10 minutes.

The original reactor vessel designed by Subhas (2017) was too small to accommodate the hydrogel samples, so a custom 40 mL glass beaker was fabricated and used instead (Figure **4.2**). The new reactor required 10 µL of isotope spike in 35 mL of buffer solution. CA-CPG beads were mechanically robust enough to withstand stirring in the reactor, but the hydrogels would break apart and leak enzyme, thereby complicating the resulting activity calculation. Hydrogels were therefore placed in a specialized housing unit made from the base of a 10 mL Falcon tube. Holes were drilled into the Falcon tube to allow the solution to flow through the housing unit during the MIMS measurement (Figure **4.2**).

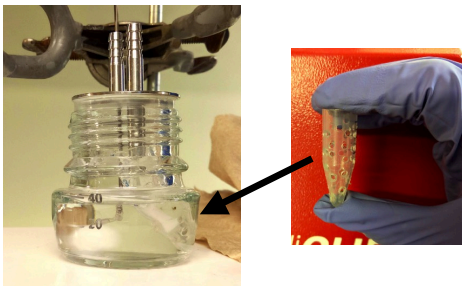

Figure 4.2: Custom 40 mL MIMS sample reactor (left) with hydrogel housing unit (right)

CA samples were systematically tested in the MIMS over time to determine the rate of activity loss. Lifetimes were assessed for samples stored only in buffer solution ("passive" conditions), and for samples placed in seawater being continuously bubbled with 10% CO_2 gas ("active" conditions). Samples were only tested under active conditions if they were shown to maintain activity under passive conditions.

4.3 Results and Discussion

4.3.1 Fluidized Bed Reactors

The results from the fluidized bed reactors are listed in Table 4.2, and plotted for the 0.25-0.5 mm size fraction experiments in Figure **4.3**. Reactors were run in pairs so that one could serve as a control while the test reactor had CA added to its water inflow stream. Bed fluidization was observed in all reactors at a gas flow rate of 5.2 L min^{-1}, in good agreement with the 5.1 L min^{-1} calculated from Eq. (4.2). Note that reactors in the lab were run with seawater bubbling 10% CO_2, while all other reactors were run with tap water. Vertical black dashed lines indicate where the flow rates of the reactors were changed. The vertical red lines in panel (C) indicate times when the reactor was reset due to pump failure and subsequent flooding of the tubing (first line), or due leaks forming in the reactor base (second line).

Table 4.2: Results from fluidized bed reactors

Flow Rate (mL min^{-1})	Rock Size (mm)	Added Alk without CA (µmol kg^{-1})	Added Alk with CA (µmol kg^{-1})	CA Benefit (µmol kg^{-1})	% Change	Extra CO_2 Captured (g yr^{-1})	Cost ($ g^{-1} extra CO_2)
Compressed Gas Tank (10% CO_2)							
5.0	1-2	2820 ± 86	-	-	-	-	-
2.5	1-2	4220 ± 133	5044 ± 50	824 ± 142	19.5 ± 3.1	23.8 ± 4.1	1465
1.0	0.25-0.5	5863 ± 163	7359 ± 141	1496 ± 216	26 ± 4	17.3 ± 2.5	800
CoGen Powerplant Smokestack (3% CO_2)							
8.0	0.25-0.5	3040 ± 59	3387 ± 26	347 ± 65	11.4 ± 2.1	32.1 ± 6.0	3,500
4.0	0.25-0.5	3327 ± 19	3537 ± 27	210 ± 33	6.3 ± 1.0	9.7 ± 1.5	5,800
2.0	0.25-0.5	3672 ± 42	3785 ± 29	113 ± 51	3.1 ± 1.4	2.6 ± 1.2	10,600
Ambient Air							
2.0	0.25-0.5	1093 ± 304	1078 ± 281	None	-	-	-

Extra CO_2 capture rate calculated by converting the "CA Benefit" at a given flow rate assuming a 2:1 Alk:CO_2 conversion

CA Cost calculated assuming price of $1876 g^{-1} (price from Worthington Biochemical Co. August 2019) and calculating the total CA used in 1 year at the designated flow rate and [CA] = 14.15 mg L^{-1}

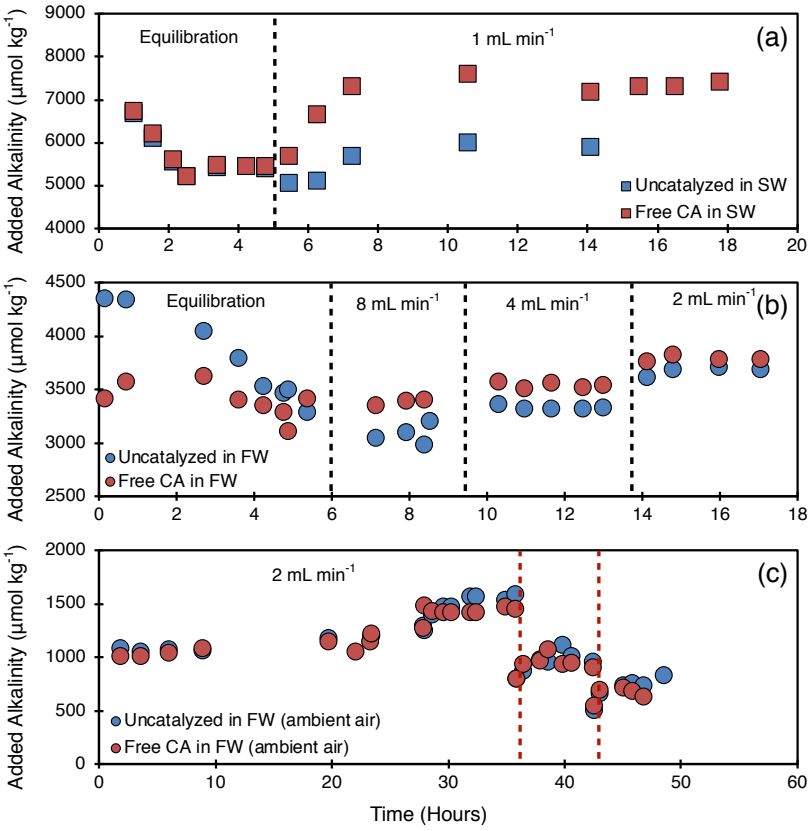

Figure 4.3: Increase in effluent alkalinity for fluidized bed reactors operating on a) 10% CO_2 in seawater (starting alk 1900 µmol kg^{-1}), b) 3% CO_2 from the Caltech powerplant smokestack in freshwater (FW, starting alk 1200 µmol kg^{-1}), c) Ambient air in freshwater. Reactors with 14 mg CA L^{-1} are in red. Dashed vertical lines indicate changes in the water inflow rate. Red vertical lines in c) indicate reactor structural failures (see text for details).

The added alkalinity (defined as alkalinity in excess of the solution starting alkalinity) for each reactor pair was proportional to the % CO_2 of the inflow gas, and inversely proportional to the water inflow rate. These trends make sense, as higher CO_2 concentrations increase the chemical driving force of the solution (decrease Ω), and lower inflow rates increase the time a volume of liquid can react with the carbonate bed. For uncatalyzed reactors dissolving in freshwater at an inflow rate of 2 mL min^{-1}, the added alkalinity increases from 1093 ± 304 to 3672 ± 42 µmol kg^{-1} when switching from ambient air (Figure **4.3**c) to 3% CO_2 (Figure **4.3**b). Although not directly comparable due to the use of seawater as opposed to freshwater,

the added alkalinity reached 5863 ± 163 μmol kg^{-1} when fluidizing reactors with 10% CO_2 in the lab (Figure **4.3**a).

After an initial equilibration period, 14.15 mg mL^{-1} CA was added to the inflow water stream of one reactor in each reactor pair**.** CA increased the effluent alkalinity by as much as 26 ± 4% in the lab (10% CO_2), and 11.4 ± 2.1% for reactors attached to the Caltech cogeneration powerplant smokestack (3% CO_2). CA had no effect when reactors were fluidized using ambient air, emphasizing the need to concentrate CO_2 to decrease Ω in real world implementations of these reactors.

The added alkalinity at a given flow rate was converted to a CO_2 capture rate by assuming a molar equivalence of 2:1 added Alk:CO_2 and using the molar mass of CO_2. For powerplant reactors, the added CO_2 that was captured when using CA followed an empirical power law dependence on the reactor overturning rate (defined as the reactor volume divided by the water inflow rate, units of hours):

$$\text{Added } CO_2 \text{ Capture}_{(gCO_2\ yr^{-1})} = 14(\text{Overturning Rate})^{-1.8} \qquad \text{Eq. (4.4)}$$

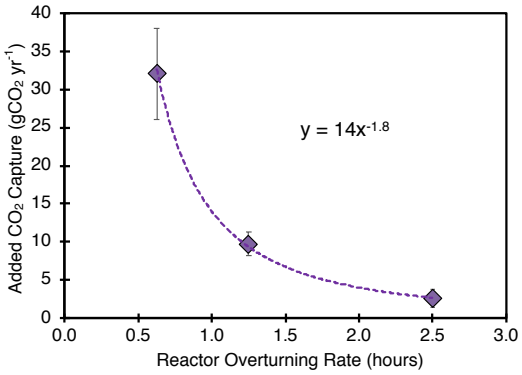

Figure 4.4: Amount of extra CO_2 captured (gCO_2 yr^{-1}) in reactors operating with 14 mg CA L^{-1} in freshwater versus the reactor overturning rate (hours, calculated from reactor volume divided by the water inflow rate). The relation follows an empirical power law dependence.

CA appears to have the largest relative effect when dissolution rates are fast, either due to low solution Ω from fast flow rates, or due to the dissolution of finer grained material. This is initially surprising considering that CA increases dissolution rates by 250x near equilibrium versus just 2x far from equilibrium (Subhas et al., 2017), but it is a reminder that Ω is the first order determinant of dissolution rates. Increased flow rates keep the reactor Ω at lower levels, allowing CA to improve upon a dissolution rate that is already quite high. The importance of Ω also explains why CA had no effect when running reactors with ambient air. The relatively low CO_2 content of ambient air did not change the solution Ω significantly, and without an overall chemical driving force to act alongside, CA could have no effect.

The data from the fluidized bed reactors demonstrate the challenges of scaling up for real world applications. In order to combat climate change effectively, a reactor must capture as much CO_2 as possible at the lowest marginal cost. Adding free CA to the reactors can boost carbon capture rates by 20+%, but CA is expensive, and the marginal cost of the captured CO_2 is on the order of several hundred dollars per gram (Table 4.2). Immobilizing CA such that it remains in the reactor offers a way to decouple the dissolution rate improvements from the prohibitively expensive cost of the enzyme.

4.3.2 Physical Immobilization of Hydrogels

CA was successfully incorporated into a wide range of hydrogels, the results of which are summarized in Table 4.3. The first iterations of hydrogels were cured as thin cylinders within 1 mL syringes using 2H2M photoinitiator (Figure **4.5**a), while subsequent trials used TPO-Li photoinitiator and higher UV strengths (Figure **4.5**b). The results for each recipe were similar. The MIMS activity assays of the cylinders showed evidence of diffusion limitation into and out of the gel (Figure **4.5**c). Compared to free CA which exhibits a linear decrease in $\ln(f^{18})$ over time (Subhas, 2017), the CA-hydrogel cylinders produced a curved slope. Activity measurements were therefore standardized by time to only include data from 200-350 seconds. Cutting the CA cylinder into smaller pieces produced activity measurements that scaled directly with the increase in surface area (Figure **4.5**d). Smaller hydrogel pieces also demonstrated less curvature in the MIMS activity assay.

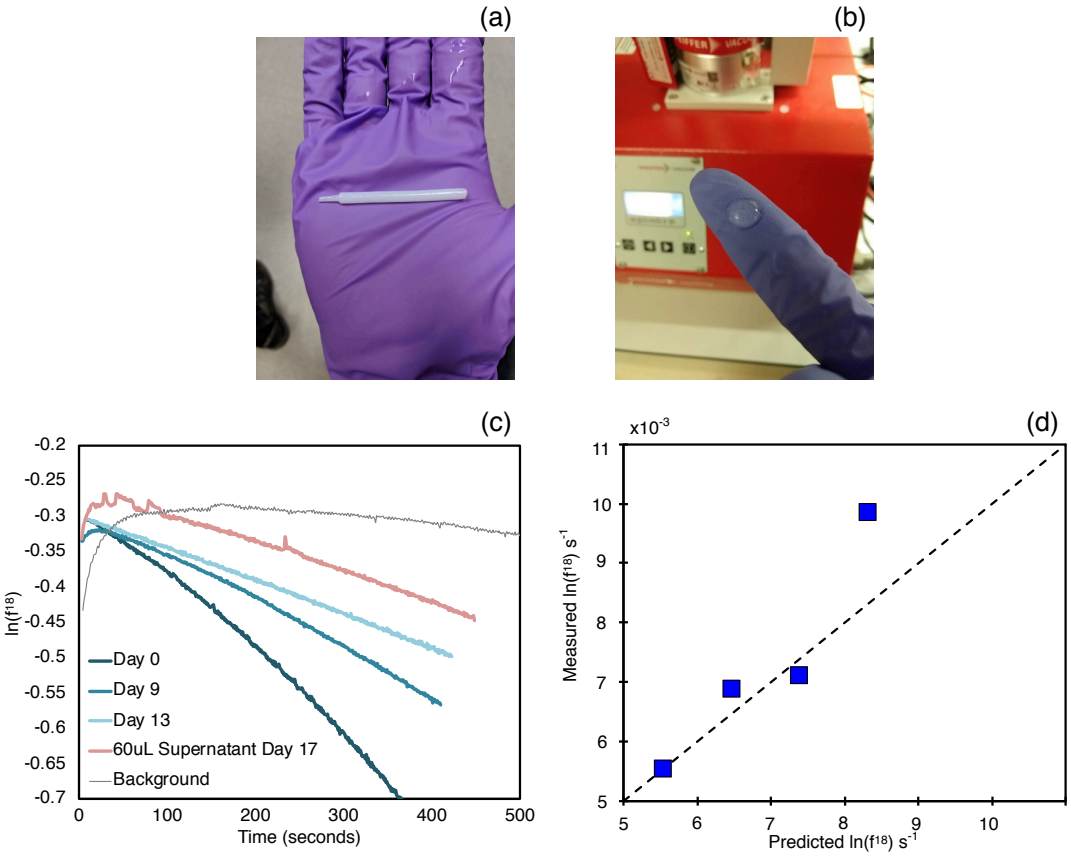

Figure 4.5: Representative CA-hydrogels a) cured in a 1 mL syringe using 2H2M photoinitiator with a $1 \cdot 10^{-3}$ W cm^{-2} 365 nm UV lamp and b) using LAP photoinitiator with a 1 W cm^{-2} 405 nm UV lamp. MIMS activity assays of c) ln(f^{18}) versus time of the same hydrogel tested over multiple days, and d) measured versus predicted activity for a hydrogel subdivided into smaller pieces. The dashed line in d) is the 1:1 measured:predicted activity based upon the increase in surface area from subdividing the hydrogel.

Table 4.3: Summary of Hydrogel Experiments						
PEGDA size (g mol^{-1})	% PEGDA	Lamp Strength (W cm^{-2})	Initiator	Activity · 10^{-3} ln(f18) s^{-1} $mgCA^{-1}$	% of Free CA Activity	Retain Activity (Y/N)?
Pure Hydrogel						
575	10	$1{\cdot}10^{-3}$	2H2M	6.2	2.1	N
		$1{\cdot}10^{-3}$	LAP	3.0	1.0	N
		0.6	**LAP**	**64**	**21**	**N**
	15	$1{\cdot}10^{-3}$	2H2M	4.8	1.6	N
	20	0.6	LAP	4.2	1.4	N
		$1{\cdot}10^{-3}$	2H2M	1.3	0.4	N
	25	$1{\cdot}10^{-3}$	2H2M	1.0	0.3	N
	30	$1{\cdot}10^{-3}$	2H2M	0.8	0.3	N
		0.6	LAP	2.8	0.9	N
	40	$1{\cdot}10^{-3}$	2H2M	0.14	0.05	N
	50	$1{\cdot}10^{-3}$	2H2M	0.10	0.03	N
5K	**12**	**1**	**LAP**	**30**	**10**	**N**
10K	**12**	**1**	**LAP**	**39**	**13**	**N**
20K	12	$1{\cdot}10^{-3}$	LAP	0.6	0.2	N
	24	$1{\cdot}10^{-3}$	LAP	0.8	0.3	N
Curing Within Porous Silicon Sheets						
575	10	$1{\cdot}10^{-3}$	LAP	2.0	0.7	N
		0.6	LAP	9.6	3.2	N
	20	0.6	LAP	1.6	0.5	N
	30	0.6	LAP	5.6	1.9	N
		$1{\cdot}10^{-3}$	LAP	2.1	0.7	N
3.4K	12	1	LAP	12	3.8	N
5K	12	1	LAP	22	7.2	N
10K	12	1	LAP	16	5.2	N
20K	12	$1{\cdot}10^{-3}$	LAP	0.2	0.7	N
	24	$1{\cdot}10^{-3}$	LAP	0.2	0.6	N

The CA-hydrogels showed promising initial activity levels, but this activity was short lived. Assaying 60 µL of storage solution produced activity levels above the background solution, indicating that the hydrogels were leaking CA (Figure **4.5**c). This was surprising, considering that previous work has shown that PEGDA sizes up to 20K g mol^{-1} should be capable of retaining a 30 kDa protein such as CA (Cruise et al., 1998). In an attempt to alleviate enzyme

leakage, we systematically increased the percentage of PEGDA relative to buffer solution (Figure **4.6**). While this increase helped the CA-hydrogels to maintain their activity for up to two weeks, the magnitude of the activity was too low to realistically be of use in a reactor. Indeed, even the best pure CA-hydrogels had an initial activity mg^{-1} that was only 10-20% of the free enzyme. This low activity level could be useable if there were no losses over time, but the activity decreased to < 1% of the original value after 2 weeks under passive storage conditions. Increasing the UV lamp intensity led to improvements in initial activity (max of $2.6 \cdot 10^{-2}$ $\ln(f^{18})$ s^{-1} $mgCA^{-1}$), but the resulting hydrogels still lost 90% activity after 2 hours and were therefore not tested over longer time periods.

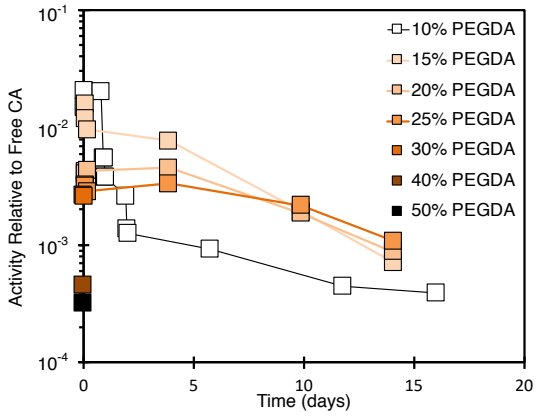

Figure 4.6: MIMS activity $mgCA^{-1}$ over time of a suite of PEGDA-575 hydrogels relative to activity mg^{-1} of free CA (hydrogel activity / free CA activity).

Another impediment to the use of CA-hydrogels in the reactors was their poor mechanical durability. Gels would break apart under moderate stirring conditions, causing faster leakage of CA into the surrounding solution.

Regardless of the aforementioned downsides, pure CA-hydrogels were introduced into a fluidized bed reactor in an effort to test if MIMS activity corresponded with dissolution catalysis. A total of 70.2 mg CA were cured into hydrogels and subdivided into 203 cylindrical pieces, each approximately 3-5 mm tall and 3-5 mm in diameter. The activity of a 15-piece subset was 0.0115 $\ln(f^{18})$ s^{-1}, so the estimated activity of all 203 pieces was 0.155

$\ln(f^{18})$ s^{-1}. This activity level was equivalent to 0.52 mg of free CA, for an effective CA concentration in the reactor of 1.73 mg L^{-1}. Although low, this amount of CA should have theoretically produced a measurable change in alkalinity. 14.15 mg L^{-1} of dissolved CA resulted in an alk increase of ~1500 μmol kg^{-1}, so assuming catalysis scales linearly with [CA], 1.73 mg CA L^{-1} should cause an increase of 183 μmol kg^{-1}, just above the ± 100 μmol kg^{-1} reproducibility of reactor alk titrations. The hydrogels were placed in a Falcon tube with pre-drilled holes (similarly to the housing unit for the MIMS assay) and suspended midway up the reactor using twine. No change in the alkalinity of the reactor effluent was observed over a period of 3 hours. Although not a definitive test due to the low effective activity of the hydrogels, it reaffirmed that large improvements would need to be developed if pure hydrogels were to be realistically implemented as reactor catalysts.

CA-PEGDA solutions were also cured within PS sheets (Table 4.3). Although this greatly improved the mechanical durability of the hydrogels, the best activity mg^{-1} that was achieved was still only 7.2% of free CA. The CA-PS-hydrogels did not show any improvement in enzyme retention.

4.3.3 Coupling CA to CPG Beads

CA-CPG beads demonstrated marked improvements in mechanical durability, activity, and activity retention relative to their CA-hydrogel counterparts. Freely dispersed CA-CPG beads ranged in activity between 11-80% activity mg^{-1} relative to free CA, depending upon the batch (Table 4.4). The density of the coupled CA-CPG beads was marginally greater than water, so the beds would stay suspended in solution for ~15-20 minutes after being dispersed. This density made the beads difficult to incorporate into reactors, as they were quickly lofted out of the reactor and clogged any filter put in their path, even at very low flow rates.

Table 4.4: Summary of CA-CPG Activity				
CA Type	Activity · 10^{-3} $\ln(f^{18})$ s^{-1} $mgCA^{-1}$	% of Free CA Activity	Lifetime (passive)	Lifetime (active)
Free CA	300	100	> 1 year	45 minutes
Dispersed CA-CPG	33.6-240*	11-80	> 6 months	> 30 hours
CA-CPG in mesh bag	12	4	> 6 months	> 30 hours
*Activity of CA-CPG beads depended upon the batch, with the highest activity mg^{-1} being 80% of free CA				

Figure 4.7: CA-CPG beads dispersed in 50 mM pH 7 phosphate buffer (left) and sealed within 70 μm mesh bags (right)

To rectify the problem of CA-CPG bead loss, beads were sealed within 70 μm pore size mesh bags (Figure **4.7**). This prevented the loss of CA-CPG beads due to lofting, but the extra diffusion limitation imposed by the bag decreased the activity of the beads by an order of magnitude, making them equivalent to CA-hydrogel activity. However, sealing the beads enabled repeated lifetime measurements of the same exact material under active conditions of bubbling with 10% CO_2 (Figure **4.8**). CA-CPG beads showed excellent activity retention under active bubbling conditions. Free CA lost all activity within 3 hours, whereas CA-CPG beads maintained 100% of their initial activity for 30 hours of active bubbling. CA-CPG beads also maintained > 50% of their initial activity for over 6 months when stored in passive conditions.

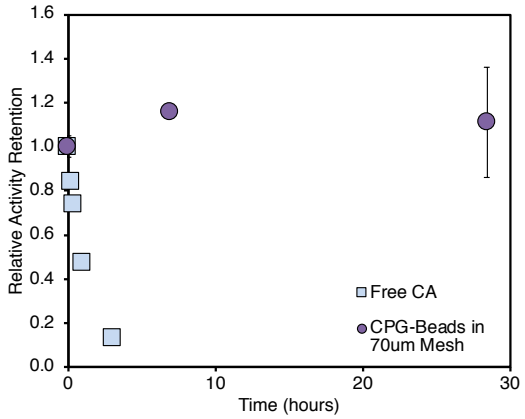

Figure 4.8: Relative activity retention (measured activity / initial activity) of free CA (squares) and CA-CPG beads in 70 μm mesh bags (circles) versus time spent in solution bubbled with 10% CO_2.

Given the excellent activity retention of CA-CPG beads, it then came to test if they could be used for dissolution catalysis. Two packed bed reactors were filled with 48 g of 1-2 mm carbonate rock and run in parallel at a water inflow rate of 3.4 mL min^{-1}. This flow rate gave a residence time of fluid in the reactor of < 10 minutes, which Eq. (4.4) implies should allow for greater relative contributions of CA to the overall alkalinity signal. After an initial equilibration period, 1 g of CA-CPG beads was mixed into the test reactor. The activity of the beads within 70 μm bags had been measured using the MIMS to be 0.12 ($ln(f^{18}) s^{-1}$) per gram. Using the measured activity of free CA of 0.3 mg^{-1}, the added beads had an activity equivalent to 0.12/0.3 = 0.4 mg of free CA. The volume of the reactor was 30 mL, so the equivalent concentration of CA was 13.4 mg L^{-1}. The activity was estimated using measurements from CA-CPG beads in bags, and therefore represents a low end estimate relative to what would be calculated using freely dispersed bead activity.

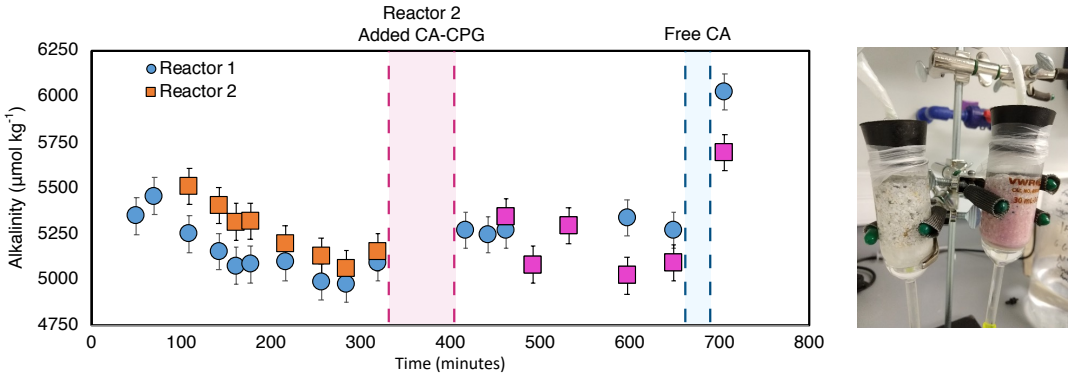

Figure 4.9: Total alkalinity versus time (left) for packed bed dissolution reactors (right). Two reactors were run in parallel at a flow rate of 3.2 mL min^{-1} of seawater. After an initial equilibration period, 1g of CA-CPG beads were mixed into Reactor 2 (pink coloring in the reactor in the right panel). When no change in alkalinity was observed, 15 mg L^{-1} of free CA was added to inflow streams of both reactors.

Beyond some alkalinity fluctuations due to recalibrating the water inflow rate, there was no difference in alkalinity between the two reactors (Figure **4.9**). To ensure that the lack of change was not due to the reactor malfunction, 15 mg L^{-1} of free CA was added to the inflow streams of each reactor. This amount was chosen was it would produce an equivalent MIMS activity as estimated for the CA-CPG beads. The free CA caused the alkalinities of each reactor to increase by ~10%, from ~ 5250 to 5900 µmol kg^{-1}.

The results from the packed bed reactors match those conducted by Dr. He (personal communications) and suggest that the mechanism of CA dissolution catalysis is via direct proton transfer from His-64 to the mineral surface, and not by an increase in the effective concentration of H_2CO_3. This mechanistic insight is consistent with results in freshwater dissolution that showed that H_2CO_3 had no effect on dissolution rates (Pokrovsky et al., 2005). It is also consistent with the mechanistic model of seawater calcite dissolution presented in Chapter 3 of this thesis, where the H_2CO_3 attack term was effectively 0.

4.4 Summary and Conclusions

We designed a fluidized bed reactor capable of sequestering CO_2 from concentrated gas streams both in the lab and directly from a powerplant smokestack. We found that freely dissolved CA catalyzed dissolution rates more effectively in reactors operating with higher % CO_2 gas streams and had no effect when bubbling in ambient air. Free CA is prohibitively expensive for use in large scale reactors, so methods were developed to retain CA within hydrogels and to chemically couple the enzyme to glass beads. Both retention techniques demonstrated activity when assessed by the MIMS, but hydrogels were mechanically fragile and lost nearly all activity after 2 weeks. CA-beads showed marked improvements in durability and maintained their activity for > 6 months, but the beads showed no catalytic effect when incorporated into packed bed dissolution reactors. These results suggest that the mechanism of CA dissolution catalysis is via direct proton transfer to the mineral surface rather than an increase in the effective concentration of H_2CO_3. These results also match both theoretical predictions made earlier in this thesis, and experimental results in freshwater (Pokrovsky et al., 2005). Enhanced dissolution of carbonate rocks remains a promising avenue to combat climate change, and catalytic materials involving direct proton transfer mechanisms should be considered in the future.